Order of lipid phases in model and plasma membranes

Hermann-Josef Kaiser[a], Daniel Lingwood[a], Ilya Levental[a], Julio L. Sampaio[a], Lucie Kalvodova[a,b], Lawrence Rajendran[a,c], and Kai Simons[a,1]

[a]Max Planck Institute of Molecular Cell Biology and Genetics, 01307 Dresden, Germany; [b]Infectious Disease Research Institute, Seattle, WA 98104; and [c]Systems and Cell Biology of Neurodegeneration, Department of Psychiatry Research, University of Zurich, 8008 Zurich, Switzerland

Contributed by Kai Simons, August 11, 2009 (sent for review May 8, 2009)

Lipid rafts are nanoscopic assemblies of sphingolipids, cholesterol, and specific membrane proteins that contribute to lateral heterogeneity in eukaryotic membranes. Separation of artificial membranes into liquid-ordered (Lo) and liquid-disordered phases is regarded as a common model for this compartmentalization. However, tight lipid packing in Lo phases seems to conflict with efficient partitioning of raft-associated transmembrane (TM) proteins. To assess membrane order as a component of raft organization, we performed fluorescence spectroscopy and microscopy with the membrane probes Laurdan and C-laurdan. First, we assessed lipid packing in model membranes of various compositions and found cholesterol and acyl chain dependence of membrane order. Then we probed cell membranes by using two novel systems that exhibit inducible phase separation: giant plasma membrane vesicles [Baumgart et al. (2007) *Proc Natl Acad Sci USA* 104:3165–3170] and plasma membrane spheres. Notably, only the latter support selective inclusion of raft TM proteins with the ganglioside GM1 into one phase. We measured comparable small differences in order between the separated phases of both biomembranes. Lateral packing in the ordered phase of giant plasma membrane vesicles resembled the Lo domain of model membranes, whereas the GM1 phase in plasma membrane spheres exhibited considerably lower order, consistent with different partitioning of lipid and TM protein markers. Thus, lipid-mediated coalescence of the GM1 raft domain seems to be distinct from the formation of a Lo phase, suggesting additional interactions between proteins and lipids to be effective.

generalized polarization value | giant unilamellar vesicle | membrane organization | lipid sorting | lipid raft

The lipid raft hypothesis postulates that selective interactions among sphingolipids, cholesterol, and membrane proteins contribute to lateral membrane heterogeneity (1). A tenet of the model is that small, dynamic cholesterol-sphingolipid-enriched assemblies can be induced to coalesce into larger, more stable structures through clustering of domain components (2). Although experimental data support cholesterol-dependent nano-scale membrane heterogeneity (3–8) and selective domain formation upon raft cross-linking (9–12), the mechanisms that govern such associations in cell membranes remain unclear.

On the molecular level, a key feature that is thought to contribute to raft assembly is the propensity of cholesterol to pack tightly with saturated acyl chains of lipids causing them to adopt an extended conformation (13, 14). In multi-component model membranes ($n > 2$), this interaction can lead to microscopically separate fluid membrane phases: the liquid-ordered (Lo) phase, enriched in saturated (sphingo-)lipids and cholesterol in a highly condensed state, and the liquid-disordered (Ld) phase, enriched in unsaturated glycerophospholipid in a disordered state (15–17).

Several features of the Lo phase in model membranes correspond to the predicted properties of lipid rafts in cell membranes (15, 18). Also in terms of protein segregation, GPI-anchored proteins, which are raft-associated in native membranes, partition into the Lo phase (19, 20). However, one difference is striking: raft-associating transmembrane (TM) proteins have been shown to be excluded (21–24), suggesting energetic constraints for TM α-helices partitioning into the tightly packed Lo phase as expected from the potential disordering effect of the amino acid side chains of the TM domain (18, 24).

In live cell membranes, segregation into microscopic Lo-like and Ld-like phases has not been observed. However, two recent studies have demonstrated that, under certain conditions, microscopic phase separation can occur in biomembranes (25–27). Baumgart and colleagues used formaldehyde membrane blebbing to generate giant plasma membrane vesicles (GPMVs), which separate into a very ordered and a disordered phase upon cooling as judged by the partitioning of typical lipid phase markers (25). As in model membranes, the ordered phase excluded all native TM proteins tested (26).

In an alternative approach, Lingwood and coworkers (27) used a cell swelling procedure to generate membrane preparations called plasma membrane spheres (PMS). By addition of cholera toxin B (CtxB), phase separation was induced by clustering of the raft ganglioside GM1 at 37 °C. Significantly, in this case, raft TM proteins were selectively enriched in the GM1 phase, whereas the transferrin receptor, used as a marker for a non-raft protein, was excluded.

As formation of a Lo-like membrane environment is predicted for lipid raft domains (15, 18, 22), we were interested in how the membrane order of plasma membrane-derived vesicles compares to Lo and Ld phases of model membranes and whether the differences in separation behavior and protein inclusivity between GPMVs and PMS are somehow reflected in the degree of lipid packing.

Lipid packing can be determined with fluorescent membrane probes such as 6-dodecanoyl-2-dimethylaminonaphthalene (Laurdan) (28–30). When integrated into the bilayer, the wavelength of the emission peak of the dye is dependent on the presence of water in the membrane. Because water penetration into the bilayer is directly related to inter-lipid spacing, Laurdan has been used to measure the degree of lipid packing (31). From the contribution of its blue emission band (I_{Ch1}) and red emission band (I_{Ch2}), the generalized polarization (GP) value can be calculated as a relative measure for membrane order (28):

$$GP = \frac{I_{Ch1} - I_{Ch2}}{I_{Ch1} + I_{Ch2}}. \quad [1]$$

GP values are obtained by spectroscopy (GP_s) or by microscopy (GP_m) and can theoretically assume values from +1 (being most ordered) and -1 (being least ordered).

Author contributions: H.-J.K. and K.S. designed research; H.-J.K., D.L., I.L., and L.R. performed research; H.-J.K., D.L., I.L., J.L.S., L.K., and K.S. analyzed data; and H.-J.K. and K.S. wrote the paper.

The authors declare no conflict of interest.

[1]To whom correspondence should be addressed. E-mail: simons@mpi-cbg.de.

This article contains supporting information online at www.pnas.org/cgi/content/full/0908987106/DCSupplemental.

BIOPHYSICS AND COMPUTATIONAL BIOLOGY

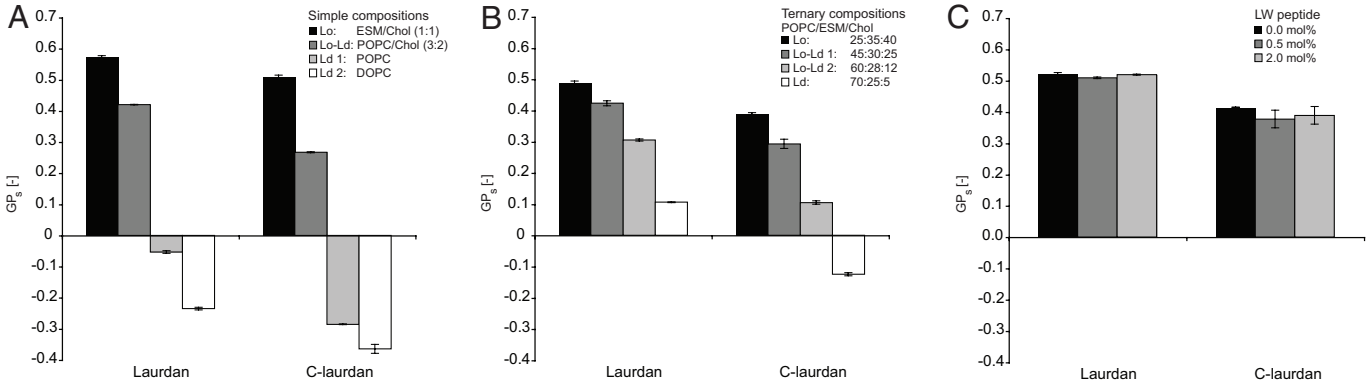

Fig. 1. GP_s analysis of pure, binary, ternary, and peptide containing LUVs representing Lo, Ld, and coexisting Lo and Ld phase. All compositions selected according to the phase diagram of de Almeida et al. (15). (*A*) GP_s values of all dyes in simple and binary model membranes of ESM-Chol (1:1), POPC-Chol (3:2), POPC, and DOPC representing Lo phase, Lo-Ld coexisting phases, and two types of Ld phase, respectively. Error bars represent SD from $n = 3$. (*B*) GP_s values of all dyes in ternary model membranes of POPC/ESM/Chol representing pure Lo (Lo: 25:35:40), 2 Lo-Ld coexisting phases (Lo-Ld 1: 45:30:25; and Lo-Ld 2: 60:28:12) and pure Ld phase (Ld: 70:25:5). Error bars represent SD from $n = 3$. (*C*) GP_s analysis of proteoliposomes. GP_s values of Laurdan and C-laurdan in model membranes (POPC/ESM/Chol 45:25:30) containing 0 mol%, 0.5 mol%, and 2.0 mol% of a synthetic TM peptide (LW peptide). Error bars represent SD from $n = 3$.

Despite its many applications in model (30, 32) and cellular membranes (29, 33, 34), Laurdan has some disadvantages on a methodological level, including low solubility in aqueous media, low fluorescence intensity, and photo-bleaching, which were overcome by the addition of a carboxyl-headgroup (6-dodecanoyl-2-methylcarboxymethylaminonaphthalene; C-laurdan) (35).

To gain better understanding about the principles of lipid-based phase separation in biomembranes, we used both Laurdan and C-laurdan to analyze lipid packing in model membranes in comparison with phase-separated GPMVs and PMS. By using fluorescence spectroscopy and microscopy, we first tested how lipid composition and a TM peptide affected the order of model membranes. We found acyl chain saturation and cholesterol to strongly increase the packing state, whereas a model TM peptide did not have an impact. When we probed the separated phases of GPMVs and PMS, increases in membrane condensation were seen for the GPMV ordered and the PMS GM1 phase. Order differences between coexisting phases were small and comparable in both systems. However, the level of packing in the temperature-dependent GPMV system was similar to model membrane Lo phase but was much greater than that observed for the GM1 phase formed in PMS. These differences in lipid packing were consistent with the partitioning behavior of lipid and TM protein markers between the phases in the plasma membrane preparations.

Results

Fluorescence Spectroscopy. ***GP_s values of Lo and Ld phases in pure and binary model membranes.*** To first estimate the packing effect of single lipid species, we analyzed simple one- and two-component lipid mixtures with known phase behavior (15). Having confirmed that Laurdan and C-laurdan partition equally between Lo and Ld membranes (Fig. S1 and Table S1), we stained large unilamellar vesicles (LUVs) and recorded emission spectra (Fig. S2). We used Lo LUVs composed of egg sphingomyelin (ESM) and cholesterol (Chol) (1:1), LUVs with coexisting Lo and Ld phases with palmitoyl-oleoyl-phosphatidylcholine (POPC)/Chol (3:2), and 2 Ld LUVs composed of pure POPC and dioleoylphosphatidylcholine (DOPC), respectively. Between the Lo-type ESM/Chol mixture and the Ld DOPC mixture, we found the biggest GP_s differences. The GP_s values of the two preparations were 0.57 ± 0.00 and -0.24 ± 0.00 for Laurdan and 0.51 ± 0.00 and -0.36 ± 0.01 for C-laurdan (Fig. 1*A*), which reflected large differences in lipid packing between pure Lo and Ld membrane phases. Compared with the Ld phase of DOPC, the Ld phase of POPC was more ordered, with -0.05 ± 0.00 for Laurdan and -0.29 ± 0.00 for C-laurdan (Fig. 1*A*), indicating that replacement of the C18:1 chain with the shorter, saturated C16:1 chain caused a considerable ordering of the Ld membrane. Moreover, Laurdan reported this change with a more pronounced GP_s shift. Addition of 40 mol% Chol to POPC results in the formation of a coexisting Lo phase (15). Accordingly, we found a strong increase in the GP_s value for this composition to 0.42 ± 0.00 for Laurdan and 0.27 ± 0.00 for C-laurdan (Fig. 1*A*) that mirrors the average GP level for coexisting Lo-Ld systems being intermediate between pure Lo and Ld phases.

GP_s values of Lo and Ld phases in ternary model membranes. Next, we analyzed ternary model membranes containing POPC, ESM, and Chol for the major lipid classes found in eukaryotic membranes. The phase behavior of this mixture has been characterized previously (15). We prepared Lo LUVs of POPC/ESM/Chol at 25:35:40 (Lo), two different types of LUVs with coexisting Lo and Ld phase with ratios of 45:30:25 (Lo-Ld 1) and 60:28:12 (Lo-Ld 2), respectively, and Ld LUVs with a ratio of 70:25:05 (Ld).

Laurdan and C-laurdan showed decreasing GP_s values for the 4 ternary compositions in the order Lo, Lo-Ld 1, Lo-Ld 2, and Ld (Fig. 1*B*), implying that that high ratios of sphingolipid-cholesterol to glycerophospholipid correlate with high membrane order.

GP_s values of ternary model membranes containing protein. As biomembranes contain high amounts of protein, we tested whether a TM peptide influenced the GP_s value. We reconstituted the synthetic LW peptide (acetyl-$K_2W_2L_8AL_8W_2K_2$-amide) at 0.5 and 2.0 mol% into LUVs of POPC/ESM/Chol 45:25:30 according to Fastenberg et al. (24). We found that the GP_s values showed only minor changes even at a high peptide-to-lipid ratio (Fig. 1*C*).

Fluorescence Microscopy. ***GP_m imaging of phase-separated model membranes.*** We then made use of the potential to measure membrane order with the dyes by two-photon microscopy. Using Lo-Ld phase-separated giant unilamellar vesicles (GUVs) of stearyl-sphingomyelin (SSM), DOPC, and Chol (2:2:1), we could obtain individual values for the coexisting phases. To visualize phase separation, we used the Ld marker lissamine-rhodamine B-dioleoylphosphatidylethanolamine (Rh-DOPE). From the blue channel (Ch1) and the red channel (Ch2) of the order-sensing dyes, artificial GP_m images (e.g., spatially resolved order maps) were calculated (see *Materials and Methods* and *SI Text*). Because of the difference between the microscopy and the spectroscopy setup, the GP_m scale was slightly broader compared with the GP_s scale.

All dyes showed a low GP_m region that overlapped with the Ld

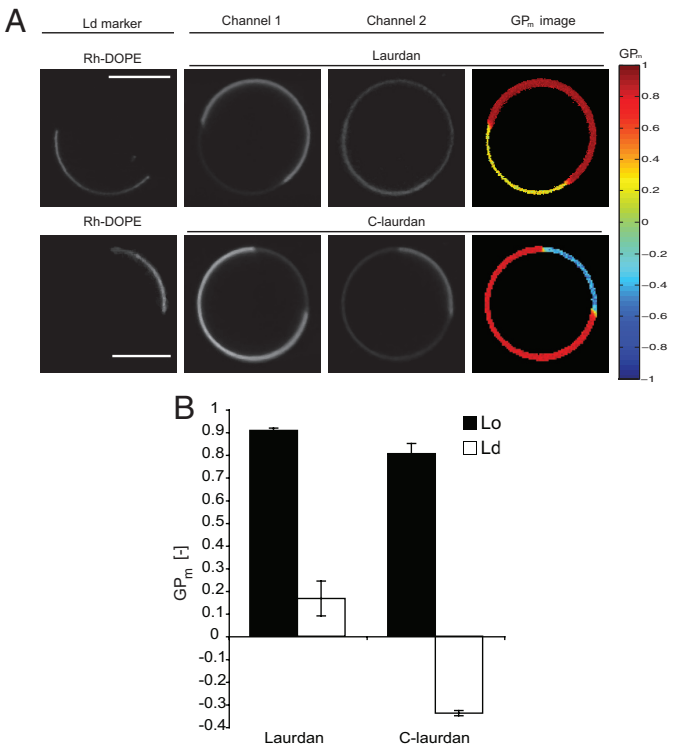

Fig. 2. GP_m analysis of Lo and Ld phase in GUVs by two-photon fluorescence microscopy using Laurdan and C-laurdan. (*A*) Phase-separated GUVs (DOPC/SSM/Chol 2:2:1) recorded in three channels (Ld marker, Ch1, Ch2) and the resulting GP_m image with a color bar indicating GP_m scale. (Scale bar, 10 μm.) (*B*) Laurdan and C-laurdan GP_m values of GUV phases as sampled from the GP_m images. Error bars represent SD from $n \geq 5$.

markers and a high GP_m region corresponding to the Lo phase (Fig. 2*A*). The GP_m values of the Lo and Ld phase were 0.91 ± 0.01 and 0.17 ± 0.08 for Laurdan and 0.81 ± 0.04 and -0.34 ± 0.01 for C-laurdan, respectively (Fig. 2*B*). As in the spectroscopy results, the order differences between Lo and Ld phase were quite large.

Marker partitioning in phase-separated plasma membrane-derived vesicles. Next, we analyzed phase-separated GPMVs and PMS to compare their properties to Lo and Ld phases of model membranes. These biomembrane systems show separation of lipids and proteins, albeit at different selectivity. We produced GPMVs and PMS from A431 cells with the methods described by Baumgart et al. (25) and Lingwood et al. (27), respectively. Cells had been transfected with the raft protein LAT TM domain carrying a monomeric red fluorescent protein (mRFP; LAT-TMD-mRFP) and were labeled with different fluorescent CtxBs, Rh-DOPE (GUVs and GPMVs), and DiD (PMS) afterward. PMS and GUVs were then imaged at 20 °C (room temperature) whereas GPMVs from A431 cells required cooling to 10 °C to phase-separate. We confirmed the findings by Sengupta et al. (26) that the Ld marker Rh-DOPE and LAT-TMD-mRFP get excluded from the GM1-enriched phase of the GPMVs marked by the CtxB label (Fig. 3 *A* and *B*). The same behavior has also been reported for GUVs (22). Strikingly, markers showed a different distribution in the PMS, where LAT-TMD-mRFP was selectively enriched in the GM1 phase but the Ld marker DiD did not show selective partitioning into either phase (Fig. 3*B*). This implied that the PMS domain containing the sphingolipid GM1 is selective for a TM raft marker and at the same time permeable to an Ld marker, whereas the GM1-enriched phase of GPMVs were neither permeable nor selectively enriched in any of the markers.

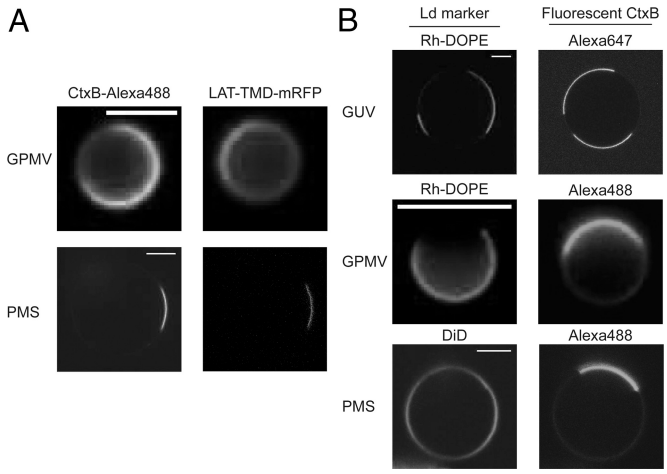

Fig. 3. Microscopy of lipid and protein marker partitioning between phases of GPMVs, PMS, and GUVs. (*A*) CtxB-labeled GM1 and the TM raft protein LAT-TMD-mRFP localize to different phases in the GPMV and to the same phase in the PMS. (Scale bar: GPMV, 5 μm; PMS, 10 μm.) (*B*) The Ld lipid marker Rh-DOPE and CtxB-labeled GM1 localize to different phases in the GUV and the GPMV. The Ld lipid marker DiD does not show a selective partitioning in the PMS between the GM1 phase and the remainder phase. (Scale bar, 10 μm.)

GP_m imaging of phase-separated plasma membrane-derived vesicles. We assessed whether the differences in marker partitioning were also reflected in the order of the phases in comparison with model membrane Lo and Ld phases. As before, we prepared GPMVs and PMSs from A431 cells. These had been stained with Laurdan and C-laurdan before vesicle induction and labeled with the phase marker CtxB-Alexa555 (PMS) or with Rh-DOPE (GPMVs) afterward. Again, PMS were imaged at 20 °C room temperature and GPMVs were cooled to 10 °C to phase-separate. Accordingly GUVs were also measured at 10 °C. To rule out a bias in the GP_m value caused by this temperature shift, we confirmed that the lipid-independent temperature effect on the dye emission lies within the error of the measurement (Fig. S3).

We found a significant difference in the order parameters between the phases, with the ordered and disordered phases of GPMVs having GP_m values of 0.70 ± 0.03 and 0.51 ± 0.04 with C-laurdan (Fig. 4 *A* and *B*) and 0.80 ± 0.01 and 0.68 ± 0.02 with Laurdan, respectively (Fig. S4 *A* and *B*). The differences between phases (i.e., ΔGP_m) were thus 0.19 ± 0.05 for C-laurdan and 0.13 ± 0.03 for Laurdan. When the GUVs were cooled down, only the Ld phase exhibited a significant change in the GP_m value. It increased by 0.04 ± 0.02 GP_m units for C-laurdan and by 0.13 ± 0.09 units for Laurdan.

We also found a significant difference in the GP_m levels between the two phases in PMS. The GM1 phase and the remaining membrane phase showed GP_ms of 0.28 ± 0.04 and 0.10 ± 0.05 with C-laurdan and 0.61 ± 0.4 and 0.54 ± 0.03 with Laurdan, respectively (Fig. 4 *C* and *D* and Fig. S4 *C* and *D*). The differences (ΔGP_m) amounted to 0.17 ± 0.06 for C-laurdan and 0.07 ± 0.05 for Laurdan. Thus, both GPMVs and PMS had a comparable small GP_m difference between the phases; however, GPMVs showed a high degree of packing similar to the Lo phase whereas PMS were significantly less ordered. To rule out that this order gap between PMS GM1 phase and the Lo phase was not merely a temperature effect, we also measured PMS at 10 °C. Even though we found a slight increase in order for both PMS phases, still, the Lo phase of GUVs was far more ordered (Fig. S5*B*). Thus, the striking result is that the raft phase in PMS is less ordered than Lo phase.

Discussion

Lateral sorting of proteins and lipids is required to generate membranes with distinct composition and function. The mecha-

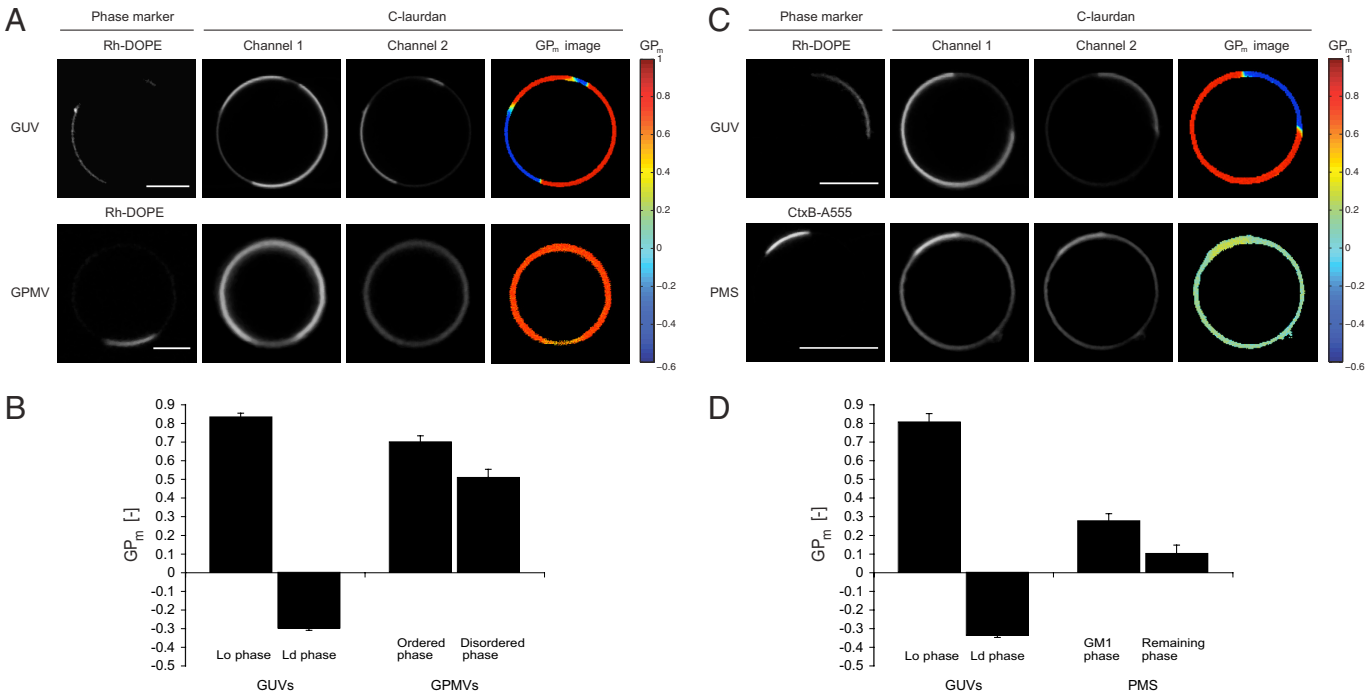

Fig. 4. GP$_m$ analysis of GUV, GPMV, and PMS phases by two-photon fluorescence microscopy using C-laurdan. (*A*) GUVs and GPMVs with two separated lipid phases recorded in three channels (phase marker, Ch1, Ch2) and the resulting GP$_m$ image with a color bar indicating GP$_m$ scale. Composition of GUVs was DOPC/SSM/Chol 2:2:1. Vesicles were imaged at 10 °C. (Scale bars: 10 μm.) (*B*) C-laurdan GP$_m$ values of GUV and GPMV phases at 10 °C (black bars) as sampled from GP$_m$ images. Error bars represent SD from $n \geq 5$. (*C*) GUVs and PMS with two separate lipid phases recorded in three channels and the resulting GP$_m$ image. Composition of GUVs was DOPC/SSM/Chol 2:2:1. Vesicles were imaged at 20 °C. (Scale bars: 10 μm.) (*D*) C-laurdan GP$_m$ values of GUV and PMS phases at 20 °C (black bars) as sampled from GP$_m$ images. Error bars represent SD from $n \geq 5$.

nisms of how cells organize lateral heterogeneity in the membrane are hardly understood. Lipid rafts—ordered assemblies of sphingolipid, cholesterol, and certain membrane proteins—are thought to be key components for the dynamic compartmentalization. Separation of model membranes into Lo and Ld phases is often considered a model for this phenomenon (15, 19); nevertheless, striking discrepancies remain (20, 22). To gain insight into potential mechanisms of raft assembly, we tested in this study how order-induced lateral segregation in model membranes compares to domain separation in plasma membrane preparations. In addition to protein and lipid markers, we made use of two order-sensing probes—Laurdan and C-laurdan—that we first compared in a systematic way.

Correlation of Model Membrane Composition and Order. In our LUV experiments, we found a strong correlation between membrane composition and order as expected (36). Increasing amounts of partially saturated lipids and cholesterol led to higher membrane packing (Fig. 1*A*). In a ternary mixture that contained representative species of the main lipid classes of eukaryotic membranes—ESM, POPC, and cholesterol—small compositional changes could be well resolved (Fig. 1*B*). This trend could also be confirmed for more complex samples such as yeast membranes (37). Moreover, GP$_s$ values were not discrete for the phase states but changed with lipid composition, decreasing in value from Lo phases to coexisting Lo-Ld phases and Ld phases (Fig. 1*B* and *SI Text*) (38). Notably, high amounts of the LW TM peptide affected membrane order only marginally in the composition tested (Fig. 1*C*), which suggests that lipid composition is the key factor to determine membrane order. Both Laurdan and C-laurdan behaved similarly. The main differences were that (*i*) the GP range is shifted to lower values with C-laurdan (Fig. 1); (*ii*) Laurdan was more sensitive in the low GP region, whereas C-laurdan discriminated packing states over the whole GP range more evenly (Figs. 1 and 2); and (*iii*) equilibration times during staining were much shorter for C-laurdan (*SI Text*).

Analysis of Phase Separation in Plasma Membranes. Our main goal in this study was to shed light on the principles that govern lipid-mediated phase separation in eukaryotic membranes, specifically focusing on the role of membrane order. Two types of plasma membrane-derived vesicles have become available to investigate inducible phase separation: GPMVs and PMS. Compared with simple model systems, these have a complex lipid and protein composition containing thousands of different lipids and membrane proteins (25, 27). Moreover, these systems lend themselves to dye-based order measurements by microscopy as a result of their micrometer-sized phases and the lack of artifacts from irregular membrane morphology (39; *SI Text*).

If cells are treated with the protein cross-linker formaldehyde, blebbing of the surface membrane into GPMVs is induced (25). Cooling to 10 °C has been shown to reversibly separate GPMVs into a highly ordered phase and a disordered phase. In agreement with other studies (25, 26), we show that the raft marker LAT-TMD-mRFP and the Ld marker Rh-DOPE enrich in the disordered phase whereas CtxB-labeled GM1 is found in the ordered phase (Fig. 3). When we then used C-laurdan and Laurdan on the vesicles, the striking result was that the measured GP$_m$ values were high (Fig. 4 and Fig. S5). At 10 °C, the ordered phase had a GP$_m$ value close to that of the Lo phase in GUVs, demonstrating that the condensation state of these two phases is very similar. Also, the disordered phase had a GP$_m$ value only 0.19 units less for C-laurdan and 0.13 units less for Laurdan. Such small GP$_m$ differences imply that the two phases separating in GPMVs are energetically close and highly miscible, in agreement with their temperature-dependent separation. Furthermore, the disordered phase exhibited a considerably higher order than pure Ld phases in simple model systems, suggesting that it is distinct from a pure Ld membrane. This high

membrane order can be related to two causes. First, as cholesterol concentration is more than 40% in plasma membranes (40, 41), not only the ordered but also the disordered phase of GPMVs likely contains considerable amounts of cholesterol, increasing the packing in the membrane. In addition, both phases are above the order of the unseparated GPMVs at 20 °C (Fig. S5*A*), indicating that the lower temperature increases the overall order in the membrane.

As our spectroscopic data show, high GP values close to the Lo level are suggestive of coexisting Lo and Ld phases (Fig. 1 *A* and *B*). As the unseparated GPMVs also displayed a high GP_m value at 20 °C (Fig. S5*A*), the vesicles probably contain pre-existing nanoscopic domains in a microscopically uniform phase as previously suggested by Baumgart et al. and others (25, 42). Indeed, recent reports propose that GPMVs have a composition close to a critical point at which a decrease in temperature coalesces pre-existing nano-domains into a microscopic phase (43).

A potential artifact of the GPMV system is that formaldehyde cross-linking likely affects the native membrane composition, presumably by formation of covalently coupled protein complexes. Lipid packing was not affected under the relevant conditions (Fig. S6). How far the chemical treatment biases the system toward the behavior observed in model membranes in which TM proteins typically become depleted from the Lo phase remains to be elucidated.

The other membrane system that we analyzed was generated by subjecting cells to hypotonic swelling (27). With this procedure, the plasma membrane forms a sphere (i.e., a PMS). A phase separation of the membrane is induced by clustering cell surface GM1 with cholera toxin at 37 °C. In contrast to Lo phases in model membranes (22) and to the ordered phase in GPMVs (26), proteins selectively partition between the PMS phases. Raft proteins (GPI-anchored, doubly acylated, or TM) are included in the GM1 phase whereas a non-raft TM protein, the transferrin receptor, is excluded. Accordingly, the LAT-TMD-mRFP is enriched in the GM1 phase. However, the Ld marker DiD does not show a selective enrichment in either phase (Fig. 3). Apparently, the lipid can easily penetrate the GM1 phase. This suggests that the partitioning criteria for proteins and lipid markers are quite different from Lo and Ld phases of model membranes. When we analyzed the order of the phases, we still found that the GM1 phase was more ordered than the remainder phase. The difference in packing between the phases measured with both C-laurdan and Laurdan was small, as with GPMVs. Strikingly, the GP_m value of the GM1 phase was significantly lower than the Lo phase in GUVs even upon cooling to 10 °C (Fig. 4 and Figs. S4 and S5), implying that the GM1 phase is not as condensed as the highly packed Lo phase of the model membrane. Considering that phase formation seen in PMS was induced at 37 °C and did not require cooling (27), our GP_m data in combination with the marker results suggest that lipid-mediated coalescence of the GM1 raft domain is distinct from the formation of a coherent Lo phase. How exactly this protein-selective GM1 domain assembles is not understood. It seems that formation of a Lo-type membrane phase by the interaction of cholesterol with saturated acyl chains is insufficient to explain domain formation on its own. Rather, the characteristics of the GM1 phase are likely to be determined by its complex lipid and protein composition. The TM raft proteins must become inherent constituents of a network of lipid-lipid and lipid-protein interactions that determine the properties of this bilayer environment.

Our studies demonstrate that the three membrane systems analyzed here represent a spectrum of different bilayer behaviors. The Lo-Ld model membrane system we used showed a striking difference in the packing density within its two phases. In contrast, the order differences between the two separating phases in GPMVs and PMSs were much smaller. It cannot be ruled out that the partial loss of membrane asymmetry dampens more pronounced differences present in native membranes (44). However, we propose that this small energetic gap in order is rather the result of the compositional complexity of the two phases in the plasma membrane preparations, as similar differences have also been reported for other domains in intact biomembranes such as the T cell synapse (45) and Golgi-derived transport vesicles (37). In addition to the interaction of cholesterol with saturated hydrocarbon chains that brings about Lo-Ld-type phase separation in model membranes, additional lateral associations come into play in cell membranes: (*i*) hydrogen bond networks mediated by the backbone chemistry of sphingolipids (1, 46–48), (*ii*) specific protein-lipid interactions (18, 49, 50), (*iii*) homo- and heterotypic protein interactions (51, 52), and (*iv*) glycan-based interaction with proteins and other glycans (53, 54). In this regard, GM1 phase formation in PMS probably involves contributions from these interactions that bring in a new quality: the selective integration of raft TM proteins. The capability of phase separation, e.g., selective de-mixing, seems to reflect an inherent property of cell membranes that probably co-evolved with increasing chemical complexity.

Materials and Methods

Reagents. POPC, DOPC, SSM, Chol, and Rh-DOPE were purchased from Avanti Polar Lipids. ESM (>80%, 16:0) and organic solvents were from Sigma-Aldrich. Laurdan, DiD, and Alexa488/647-labeled cholera toxin were from Invitrogen. C-laurdan was a gift from Dr. B. R. Cho (Seoul, Korea). Laurdan and C-laurdan stocks were prepared in ethanol and DMSO. LW peptide (acetyl-$K_2W_2L_8AL_8W_2K_2$-amide) was a gift from Dr. E. London (Stony Brook, NY). All stock concentrations of dyes were determined by spectroscopy and all lipid stocks by phosphate assay or cholesterol assay (Invitrogen).

Preparation of LUVs. LUVs were prepared according to Kalvodova et al. (21) as described in the *SI Text*. For proteoliposomes, 0.5 and 2.0 mol% of peptide was added to the lipid mixture before drying.

Preparation of GUVs. GUVs were prepared according to Bagatolli et al. (55) or Bacia et al. (56) as described in the *SI Text*, and stained with DiD or Rh-DOPE each at 0.1 mol%, and Laurdan or C-laurdan at 0.5 mol%. Alternatively, vesicles were stained with Laurdan or C-laurdan for 1.5 h at 0.4 μM after electroformation. Fluorescent CtxB was added to GUVs at 1 μg/mL after preparation.

Staining of LUVs with Fluorescent Probes. To determine the GP_s values, concentrations of 250 nM Laurdan and 100 nM C-laurdan were used on 200 μM lipid. Samples were incubated for 12 h at room temperature to equilibrate before the measurement.

Fluorescence Spectroscopy and Analysis. All spectra were recorded with 1 nm resolution on a Fluoromax-3 fluorescence spectrometer (Horriba) with a Thermo-Haake thermostat at 23 °C. Excitation wavelengths for Laurdan and C-laurdan was 385 nm. All spectra were recorded twice, averaged, and background subtracted. The GP_s values for Laurdan and C-laurdan were calculated from the following emission bands: (Ch1) 400–460 nm and (Ch2) 470–530 nm according to Eq. **1** taken from Parasassi et al. (28).

Two-Photon, Confocal Fluorescence, and Wide-Field Microscopy. All images for Laurdan and C-laurdan were recorded on a Bio-Rad two-photon setup with a Mira 2000 two-photon laser and a 543-nm laser line using a ×60 WI objective (NA 1.2). Laurdan and C-laurdan were excited at 800 nm and the emission captured using 425/50 (Ch1-low λ) and 525/70 (Ch1-high λ) filters. The markers Rh-DOPE and CtxB-Alexa555 were excited at 543 nm and detected using a LP 590 filter (see *SI Text*). 5 mM Laurdan and C-laurdan in DMSO was measured to calibrate the channels. For confocal microscopy of markers in the GUVs and PMS, a Zeiss LSM 510 inverted setup with the appropriate filters and a ×63 oil-immersion objective was used. For imaging of markers in the GPMVs, a Zeiss inverted wide-field CCD microscope with appropriate filter sets and a ×40 air objective was used. Microscopy was carried out at 20 °C. For imaging GUVs and GPMVs at 10 °C, samples were cooled on stage using a Thermo-Haake thermostat. The temperature effect on GP stability in this range was within the experimental error (Fig. S4).

Image Analysis. Image processing and analysis was carried out using Matlab R2006B (Mathworks). All images were recorded in 8-bit format, normalized, and background corrected. GP_m images were computed according to the following:

$$GP_m = \frac{I_{Ch1} - G \times I_{Ch2}}{I_{Ch1} + G \times I_{Ch2}} \quad [2]$$

where the G-factor served to calibrate the channels (29). Pixels below 20% (or less) of the maximum signal of the image ($I_i = I_{i,Ch1} + I_{i,Ch2}$) were masked black in the GP_m images and not considered for further analysis. GP_m images were displayed as 2-fold binned heat maps as indicated next to the images. Fluorescence images are depicted smoothed (i.e., median-filter) and contrast enhanced using ImageJ software (National Institutes of Health).

For sampling phase order, three GP_m areas were chosen as regions of interest (3×3 px $< A < 9 \times 9$ px) per domain and averaged. Multiple measurements ($n \geq 5$) were averaged and SDs calculated.

Cell Culture and Preparation of Plasma Membrane-Derived Vesicles. A431 cells were cultured in DMEM (4.5 g/L glucose, glutamine, penicillin, streptomycin, 10% FCS). GPMVs were produced as described in Baumgart et al. (25). PMS were generated according to Lingwood et al. (27). For the GPMVs, vesicles were stained after harvesting with 20 μM Laurdan, 20 μM C-laurdan, and 4 μM Rh-DOPE. For the PMS, Laurdan and C-laurdan were complexed to 0.05% BSA in PBS at 20 μM and fed to cells for 10 min before PMS formation.

ACKNOWLEDGMENTS. We thank P. Schwille and J. Ries (University of Technology, Dresden, Germany) for critical reading of the manuscript and the Simons laboratory for helpful discussion. We also thank B. R. Cho for supplying C-laurdan and E. London for providing the LW peptide. This work was supported by EU FP6 ''PRISM'' Grant LSHB-CT2007–037740, DFG ''Schwerpunktprogramm 1175,'' and BMBF ''BioChance Plus'' Grant 0313827. H.-J.K. received a predoctoral stipend from the Max Planck Institute.

1. Simons K, Ikonen E (1997) Functional rafts in cell membranes. *Nature* 387:569–572.
2. Hancock JF (2006) Lipid rafts: contentious only from simplistic standpoints. *Nat Rev Mol Cell Biol* 7:456–462.
3. Pralle A, Keller P, Florin EL, Simons K, Horber JK (2000) Sphingolipid-cholesterol rafts diffuse as small entities in the plasma membrane of mammalian cells. *J Cell Biol* 148:997–1008.
4. Lenne PF, et al. (2006) Dynamic molecular confinement in the plasma membrane by microdomains and the cytoskeleton meshwork. *EMBO J* 25:3245–3256.
5. Suzuki KG, et al. (2007) GPI-anchored receptor clusters transiently recruit Lyn and G alpha for temporary cluster immobilization and Lyn activation: single-molecule tracking study 1. *J Cell Biol* 177:717–730.
6. Goswami D, et al. (2008) Nanoclusters of GPI-anchored proteins are formed by cortical actin-driven activity. *Cell* 135:1085–1097.
7. Eggeling C, et al. (2008) Direct observation of the nanoscale dynamics of membrane lipids in a living cell. *Nature* 457:1159–1162.
8. Suzuki KG, Fujiwara TK, Edidin M, Kusumi A (2007) Dynamic recruitment of phospholipase C gamma at transiently immobilized GPI-anchored receptor clusters induces IP3-Ca2+ signaling: single-molecule tracking study 2. *J Cell Biol* 177:731–742.
9. Harder T, Scheiffele P, Verkade P, Simons K (1998) Lipid domain structure of the plasma membrane revealed by patching of membrane components. *J Cell Biol* 141:929–942.
10. Nicholson TB, Stanners CP (2006) Specific inhibition of GPI-anchored protein function by homing and self-association of specific GPI anchors. *J Cell Biol* 175:647–659.
11. Paladino S, Sarnataro D, Tivodar S, Zurzolo C (2007) Oligomerization is a specific requirement for apical sorting of glycosyl-phosphatidylinositol-anchored proteins but not for non-raft-associated apical proteins. *Traffic* 8:251–258.
12. Zech T, et al. (2009) Accumulation of raft lipids in T-cell plasma membrane domains engaged in TCR signalling. *EMBO J* 28:466–76.
13. Vist MR, Davis JH (1990) Phase equilibria of cholesterol/dipalmitoylphosphatidylcholine mixtures: 2H nuclear magnetic resonance and differential scanning calorimetry. *Biochemistry* 29:451–464.
14. Ipsen JH, Karlstrom G, Mouritsen OG, Wennerstrom H, Zuckermann MJ (1987) Phase equilibria in the phosphatidylcholine-cholesterol system. *Biochim Biophys Acta* 905:162–172.
15. de Almeida RF, Fedorov A, Prieto M (2003) Sphingomyelin/phosphatidylcholine/cholesterol phase diagram: boundaries and composition of lipid rafts. *Biophys J* 85:2406–2416.
16. Mouritsen OG, Zuckermann MJ (2004) What's so special about cholesterol? *Lipids* 39:1101–1113.
17. Veatch SL, Keller SL (2002) Organization in lipid membranes containing cholesterol. *Phys Rev Lett* 89:268101.
18. Simons K, Vaz WL (2004) Model systems, lipid rafts, and cell membranes. *Annu Rev Biophys Biomol Struct* 33:269–295.
19. Dietrich C, Volovyk ZN, Levi M, Thompson NL, Jacobson K (2001) Partitioning of Thy-1, GM1, and cross-linked phospholipid analogs into lipid rafts reconstituted in supported model membrane monolayers. *Proc Natl Acad Sci USA* 98:10642–10647.
20. Kahya N, Brown DA, Schwille P (2005) Raft partitioning and dynamic behavior of human placental alkaline phosphatase in giant unilamellar vesicles. *Biochemistry* 44:7479–7489.
21. Kalvodova L, et al. (2005) Lipids as modulators of proteolytic activity of BACE: involvement of cholesterol, glycosphingolipids, and anionic phospholipids in vitro. *J Biol Chem* 280:36815–36823.
22. Hammond AT, et al. (2005) Crosslinking a lipid raft component triggers liquid ordered-liquid disordered phase separation in model plasma membranes. *Proc Natl Acad Sci USA* 102:6320–6325.
23. Bacia K, Schuette CG, Kahya N, Jahn R, Schwille P (2004) SNAREs prefer liquid-disordered over ''raft'' (liquid-ordered) domains when reconstituted into giant unilamellar vesicles. *J Biol Chem* 279:37951–37955.
24. Fastenberg ME, Shogomori H, Xu X, Brown DA, London E (2003) Exclusion of a transmembrane-type peptide from ordered-lipid domains (rafts) detected by fluorescence quenching: extension of quenching analysis to account for the effects of domain size and domain boundaries. *Biochemistry* 42:12376–12390.
25. Baumgart T, et al. (2007) Large-scale fluid/fluid phase separation of proteins and lipids in giant plasma membrane vesicles. *Proc Natl Acad Sci USA* 104:3165–3170.
26. Sengupta P, Hammond A, Holowka D, Baird B (2008) Structural determinants for partitioning of lipids and proteins between coexisting fluid phases in giant plasma membrane vesicles. *Biochim Biophys Acta* 1778:20–32.
27. Lingwood D, Ries J, Schwille P, Simons K (2008) Plasma membranes are poised for activation of raft phase coalescence at physiological temperature. *Proc Natl Acad Sci USA* 105:10005–10010.
28. Parasassi T, De Stasio G, d'Ubaldo A, and Gratton E (1990) Phase fluctuation in phospholipid membranes revealed by Laurdan fluorescence. *Biophys J* 57:1179–1186.
29. Gaus K, Zech T, Harder T (2006) Visualizing membrane microdomains by Laurdan 2-photon microscopy. *Mol Membr Biol* 23:41–48.
30. Nyholm T, Nylund M, Soderholm A, Slotte JP (2003) Properties of palmitoyl phosphatidylcholine, sphingomyelin, and dihydrosphingomyelin bilayer membranes as reported by different fluorescent reporter molecules. *Biophys J* 84:987–997.
31. Bagatolli LA, Parasassi T, Fidelio GD, Gratton E (1999) A model for the interaction of 6-lauroyl-2-(N,N-dimethylamino)naphthalene with lipid environments: implications for spectral properties. *Photochem Photobiol* 70:557–564.
32. Parasassi T, De Stasio G, Ravagnan G, Rusch RM, Gratton E (1991) Quantitation of lipid phases in phospholipid vesicles by the generalized polarization of Laurdan fluorescence. *Biophys J* 60:179–189.
33. Romer W, et al. (2007) Shiga toxin induces tubular membrane invaginations for its uptake into cells. *Nature* 450:670–675.
34. Parasassi T, Loiero M, Raimondi M, Ravagnan G, Gratton E (1993) Absence of lipid gel-phase domains in seven mammalian cell lines and in four primary cell types. *Biochim Biophys Acta* 1153:143–154.
35. Kim HM, et al. (2007) A two-photon fluorescent probe for lipid raft imaging: C-Laurdan. *Chembiochem* 8:553–559.
36. Parasassi T, Di Stefano M, Loiero M, Ravagnan G, Gratton E (1994) Influence of cholesterol on phospholipid bilayers phase domains as detected by Laurdan fluorescence. *Biophys J* 66:120–132.
37. Klemm RW, et al. (2009) Segregation of sphingolipids and sterols during formation of secretory vesicles at the trans-Golgi network. *J Cell Biol* 185:601–612.
38. Parasassi T, Gratton E (1995) Membrane lipid domains and dynamics as detected by Laurdan fluorescence. *J Fluorescence* 5:59–69.
39. Parasassi T, Gratton E, Yu WM, Wilson P, Levi M (1997) Two-photon fluorescence microscopy of laurdan generalized polarization domains in model and natural membranes. *Biophys J* 72:2413–2429.
40. van Meer G, Voelker DR, Feigenson GW (2008) Membrane lipids: where they are and how they behave. *Nat Rev Mol Cell Biol* 9:112–124.
41. Chan R, et al. (2008) Retroviruses human immunodeficiency virus and murine leukemia virus are enriched in phosphoinositides. *J Virol* 82:11228–11238.
42. Feigenson GW (2009) Phase diagrams and lipid domains in multicomponent lipid bilayer mixtures. *Biochim Biophys Acta* 1788:47–52.
43. Veatch SL, et al. (2008) Critical fluctuations in plasma membrane vesicles. *ACS Chem Biol* 3:287–293.
44. Cheng HT, Megha, London E (2009) Preparation and properties of asymmetric vesicles that mimic cell membranes: effect upon lipid raft formation and transmembrane helix orientation. *J Biol Chem* 284:6079–6092.
45. Gaus K, Chklovskaia E, Fazekas de St Groth B, Jessup W, Harder T (2005) Condensation of the plasma membrane at the site of T lymphocyte activation. *J Cell Biol* 171:121–131.
46. Abrahamsson S, Dahlén B, Löfgren H, Pascher I, Sundell S (1977) Molecular arrangement and conformation of lipids of relevance to membrane structure. *Structure of Biological Membranes*, eds. Abrahamsson S, Pascher I (New York, Plenum), pp 1–21.
47. Boggs JM (1987) Lipid intermolecular hydrogen bonding: influence on structural organization and membrane function. *Biochim Biophys Acta* 906:353–404.
48. Simons K, van Meer G (1988) Lipid sorting in epithelial cells. *Biochemistry* 27:6197–6202.
49. Cherezov V, et al. (2007) High-resolution crystal structure of an engineered human beta2-adrenergic G protein-coupled receptor. *Science* 318:1258–1265.
50. Miljan EA, Bremer EG (2002) Regulation of growth factor receptors by gangliosides. *Sci STKE* 2002:RE15.
51. Engelman DM (2005) Membranes are more mosaic than fluid. *Nature* 438:578–580.
52. Scott FL, et al. (2008) The Fas-FADD death domain complex structure unravels signalling by receptor clustering. *Nature* 457:1019–1022.
53. Boggs JM, Menikh A, Rangaraj G (2000) Trans interactions between galactosylceramide and cerebroside sulfate across apposed bilayers. *Biophys J* 78:874–885.
54. Hakomori SI (2002) Inaugural article: the glycosynapse. *Proc Natl Acad Sci USA* 99:225–232.
55. Bagatolli LA, Gratton E (2000) A correlation between lipid domain shape and binary phospholipid mixture composition in free standing bilayers: a two-photon fluorescence microscopy study. *Biophys J* 79:434–447.
56. Bacia K, Schwille P, Kurzchalia T (2005) Sterol structure determines the separation of phases and the curvature of the liquid-ordered phase in model membranes. *Proc Natl Acad Sci USA* 102:3272–3277.